



UNIVERSITY OF LEEDS

This is a repository copy of *Scattering in InAs/GaSb Coupled Quantum Wells as a Probe of Higher Order Subband Hybridisation*.

White Rose Research Online URL for this paper:

<https://eprints.whiterose.ac.uk/162072/>

Version: Accepted Version

Article:

Knox, C orcid.org/0000-0002-4673-5649, Li, L orcid.org/0000-0003-4998-7259, Rosamond, M et al. (2 more authors) (2020) Scattering in InAs/GaSb Coupled Quantum Wells as a Probe of Higher Order Subband Hybridisation. *Physical Review B: Condensed Matter and Materials Physics*, 102 (4). ISSN 1098-0121

<https://doi.org/10.1103/PhysRevB.102.045310>

©2020 American Physical Society. This is an author produced version of a paper published in *Physical Review B: covering condensed matter and materials physics*. Uploaded in accordance with the publisher's self-archiving policy.

Reuse

Items deposited in White Rose Research Online are protected by copyright, with all rights reserved unless indicated otherwise. They may be downloaded and/or printed for private study, or other acts as permitted by national copyright laws. The publisher or other rights holders may allow further reproduction and re-use of the full text version. This is indicated by the licence information on the White Rose Research Online record for the item.

Takedown

If you consider content in White Rose Research Online to be in breach of UK law, please notify us by emailing eprints@whiterose.ac.uk including the URL of the record and the reason for the withdrawal request.



eprints@whiterose.ac.uk
<https://eprints.whiterose.ac.uk/>

Scattering in InAs/GaSb Coupled Quantum Wells as a Probe of Higher Order Subband Hybridisation

C. S. Knox^{1,2,*}, L.H. Li¹, M.C. Rosamond¹, E.H. Linfield¹, and C.H. Marrows²

¹ *School of Electronic and Electrical Engineering,
University of Leeds, Leeds LS2 9JT, United Kingdom*

² *School of Physics and Astronomy,
University of Leeds, Leeds LS2 9JT, United Kingdom*

(Dated: May 5, 2020)

Abstract

We have performed a detailed investigation into the inter-subband scattering within InAs/GaSb coupled quantum wells in the electron dominated regime. By considering the carrier mobilities and the quantum lifetime as a function of carrier density, we find that the occupation of higher order electron-like subbands are inhibited by anticrossing with the hole subbands. We also find that, by applying a gate bias to the GaSb layer, we are able to move the electron-hole anticrossing point in energy, modulating the electron-like states that should be localised within the InAs layer.

I. INTRODUCTION

The InAs/GaSb heterojunction has attracted a great deal of experimental interest in recent years^{1,2}. Specifically, the staggered, type II, band alignment allows the engineering of heterostructures with adjustable band alignments³, where the band gap can be tuned from a conventional semiconducting state, through a semimetallic state, into an “inverted” state, in which the principal electron and hole subbands anticross. This leads to a hybridisation gap, with the size of the band gap being dependent on the coupling between the two material systems^{4,5}.

This hybridisation gap has been predicted to give rise to the quantum spin Hall effect^{6–8}, where transport is dominated by spin filtered edge modes that bridge the topologically non-trivial band gap. However, unlike in HgTe/CdTe quantum wells (also predicted to exhibit the quantum spin Hall effect)^{9,10}, the Fermi energy is not pinned mid-gap, but is instead pinned deep within the InAs electron-like bands¹¹. As such, in order to probe this topologically interesting regime, a gate bias must be applied to the heterostructure^{12–14}. The intrinsic carrier density in the GaSb layer is approximately^{1,12,15,16} $(0.6–2) \times 10^{11} \text{ cm}^{-2}$. Previous work on double GaAs/ $\text{Al}_x\text{Ga}_{1-x}\text{As}$ quantum wells shows that a carrier density greater than $0.7 \times 10^{11} \text{ cm}^{-2}$ in a lower well can efficiently screen an upper quantum well from the action of a bottom gate¹⁷. Hence, the electric field produced by a gate bias applied to the GaSb layer should have a dominant effect on that layer, and be screened from the InAs layer. However, when InAs/GaSb coupled quantum wells are within an electron dominated regime, it has been observed that applying a gate bias to a GaSb layer within these coupled quantum well structures in fact modulates the density of electron-like states, which should be localised within the InAs layer^{12,13}.

In this paper we report a detailed study on how a gate bias affects the bandstructure of a coupled InAs/GaSb quantum well structure. Most studies of this material system have focused on the hybridisation gap formed between the principal electron-like and hole-like subbands^{1,13,15}. However, $\mathbf{k}\cdot\mathbf{p}$ calculations of wide InAs/GaSb quantum wells^{4,18} and of InAs/GaSb core/shell nanowires¹⁹ predict the existence of multiple anticrossings⁵. Here, we report that the occupation of the second, electron-like, subband is inhibited by the hybridisation gap formed between itself and the highest energy heavy-hole subband. Scattering between the principal electron-like subband and the new, hybridised, subband is probed

through in-plane magnetoresistance measurements, and a study of the quantum lifetime of charge carriers is undertaken as a function of gate bias. We also examine the Hall mobility as a function of both top and bottom gate bias, and conclude that a gate bias applied to the GaSb layer will move the anticrossing point between the electron and hole-like subbands in energy, and thus modulate the number of electron-like states within the hybridised, electron-like subbands.

II. EXPERIMENT AND ANALYSIS

The layer structure of the InAs/GaSb coupled quantum well studied here is shown in Fig. 1a. The heterostructure was grown by solid source molecular beam epitaxy, in the [001] direction on a (001) GaSb substrate. The coupled quantum well consisted of a 15 nm thick InAs channel grown on top of a 8 nm thick GaSb channel, surrounded by 50 nm thick AlSb barriers and capped with 3 nm of GaSb. These well widths were chosen so that the coupled well system should be in an “inverted” state in the absence of a gate bias^{5,8,11}. The coupled quantum well structure was then patterned into 50 μm wide Hall bars, with a 250 μm separation between probe arms by wet chemical etching²⁰. Cr/Au ohmic contacts were subsequently deposited by thermal evaporation, followed by a Cr/Au global bottom gate electrode. A 30 nm thick Al_2O_3 top gate dielectric was then deposited at 200 °C by atomic layer deposition before, finally, a Cr/Au top gate electrode was formed by thermal evaporation. An optical micrograph of a typical device is shown in Fig. 1b. Measurements were undertaken in a continuous flow helium cryostat, using standard lock-in techniques, with a source-drain bias current of 0.5 μA at a frequency of 119.77 Hz.

Measurements of the Hall carrier density and mobility were taken by sweeping the magnetic field between ± 0.2 T, for a range of top and bottom gate biases between $V_{\text{tg}} = \pm 2.5$ V (at higher top gate biases, the carrier density exhibits significant hysteresis) and $V_{\text{bg}} = \pm 3$ V (at higher biases, the bottom gate starts to leak) at a fixed temperature of 1.5 K. The results of these measurements (Fig. 2), show that the top and bottom gates both modulate the Hall carrier density of electron-like carriers as if they were modulating a single InAs well, where a negative bias across either gate depletes electron-like carriers, whilst a positive bias excites them. Additionally, at all gate biases, there is no bending in the low-field Hall resistance, indicating that the transport is dominated by a single, electron-like, carrier gas²¹.

If we model the gates simplistically as parallel plate capacitors with a constant dielectric constant of 11 (the average dielectric constant, ϵ , of the stack structure at 300 K²²), we find that the top gate appears to be 111 ± 2 nm away from the channel at all bottom gate biases. This value is comparable with the physical gate-channel separation of 95 nm, taking into account the 30 nm Al₂O₃ dielectric, the 3 nm thick GaSb cap, the 50 nm thick AlSb top barrier and the 15 nm thick InAs channel. When similar analysis is performed with the bottom gate, the channel appears to be 1100 ± 200 nm away from the bottom gate, which is consistent with the 1000 nm thick Al_{0.8}Ga_{0.2}Sb buffer layer. The overestimation of the gate-channel separation is to expected, due to the lower value of ϵ at cryogenic temperatures²³.

At low carrier densities, the Hall mobility depends solely on the Hall carrier density, regardless of the combination of top and bottom gate voltages used to obtain that carrier density, as shown in Fig. 2c. We also note that, at the lowest carrier densities, the Hall mobility follows a simple power law scaling with the total carrier density, where $\mu \propto n^{1.31 \pm 0.05}$, highlighted in Fig. 2c by a dashed red line. This would indicate that the conduction within this coupled quantum well system is limited by scattering from remote ionised impurities^{24–26}. As the carrier density is increased, the two-dimensional electron gas (2DEG) provides greater screening against this impurity potential, leading to an increase in the Hall mobility. We can see from Fig. 2c, however, that there is a clear peak in the Hall mobility at a Hall carrier density of $(15.9 \pm 0.2) \times 10^{11}$ cm⁻². Additionally, the Hall carrier density alone continues to determine the mobility, and thus the nature of the scattering, within this heterostructure up until a carrier density of $(20.8 \pm 0.2) \times 10^{11}$ cm⁻². At carrier densities higher than this, a more negative bottom gate bias results in a lower Hall mobility for a comparable carrier density, highlighted with an arrow in Fig. 2c. This implies that at carrier densities higher than $(20.8 \pm 0.2) \times 10^{11}$ cm⁻², the top and bottom gates have different effects on the transport. It is also at this Hall carrier density that we start to see SdH oscillations in the high field magnetotransport that are no longer bound by a single envelope function (shown in Fig. 3a), indicating that there is an additional 2D carrier gas contributing to transport²⁷.

We note that the peak in the Hall mobility at a carrier density of $(15.9 \pm 0.2) \times 10^{11}$ cm⁻² is qualitatively similar to that seen in single InAs quantum wells²⁶, where a drop in Hall mobility occurs as a second electron subband is populated. However, if the drop in Hall mobility observed in Fig. 2c was simply due to inter-subband scattering, we would expect the occupation of the first subband to saturate at the peak in the Hall mobility²⁷. To test

this, we took Fourier transforms of the Shubnikov de-Haas (SdH) oscillations up to 8 T at a constant temperature of 1.5 K, over a range of top gate biases (shown in Fig. 3a), and compared the carrier density extracted from the Fourier spectrum of the SdH oscillations to the Hall carrier density. The results of this study are shown in Fig 3b, with the Hall mobility shown in purple, for comparison. Below a Hall carrier density of $(18.5 \pm 0.2) \times 10^{11} \text{ cm}^{-2}$, the Hall carrier density increases linearly with increasing top gate bias, until $V_{\text{tg}} = -0.25 \text{ V}$, where there is a slight reduction from the linear increase, indicative of the presence of a second carrier species with a lower mobility²⁷.

We find that the carrier density, extracted from the Fourier transform of the SdH oscillations up to 4 T, is experimentally identical to that extracted from the low field ($B \leq 0.2 \text{ T}$) Hall coefficient for Hall carrier densities below $(21.7 \pm 0.2) \times 10^{11} \text{ cm}^{-2}$ (below $V_{\text{tg}} = +0.6 \text{ V}$). We note that $(21.7 \pm 0.2) \times 10^{11} \text{ cm}^{-2}$ is also the carrier density at which we start to see SdH oscillations no longer bound by a single envelope function, as shown in Fig 3a. At the higher Hall carrier density of $(23.5 \pm 0.2) \times 10^{11} \text{ cm}^{-2}$ (at $V_{\text{tg}} = +0.9 \text{ V}$), we start to observe a new peak in the Fourier spectrum, with the related carrier density shown in Fig 3b in red, indicating a significant number of carriers occupying a second, electron-like subband. Taking a linear fit of this second, electron-like, carrier density as a function of top gate bias (shown in Fig. 3b by a dashed blue line), we would expect this new subband to be populated at a Hall carrier density of $(20.0 \pm 0.2) \times 10^{11} \text{ cm}^{-2}$ (at $V_{\text{tg}} = +0.15 \text{ V}$), which is remarkably similar to the carrier density at which we observe SdH oscillations no longer bound by a single envelope function, $(21.7 \pm 0.2) \times 10^{11} \text{ cm}^{-2}$.

For clarity, Fig. 3c shows the quantum Hall plateaux and SdH oscillations at a carrier density of $(18.4 \pm 0.2) \times 10^{11} \text{ cm}^{-2}$. We can see that the SdH oscillations arise from a single envelope function, and that the quantum Hall plateaux align well with the expected plateaux for even filling factors ($< 5\%$ deviation from integer fractions of the von Klitzing constant). There is no bending in the low-field Hall trace, and neither are there any plateaux that arise at odd-integer fractions of the von Klitzing constant at low fields²⁸, which would indicate a significant parallel conduction channel or significant population of a second occupied subband. We do note, however, that there is a small positive magnetoresistance at all gate biases, and that the SdH oscillations do not reach $0 \text{ } \Omega$ resistance. This may point to a parallel conduction channel, albeit one occupied by a small number of carriers with a low mobility.

We also took Fourier transforms of the SdH oscillations at various bottom gate biases at 1.5 K, when the top gate is grounded. The majority of the SdH oscillations should arise from the most mobile carrier within the system, and so the carrier density derived from these oscillations should also deviate from the Hall carrier density if a second carrier gas is modulated by action of a bottom gate. The results of this study are shown in Fig. 3d. We can see that both carrier densities show remarkably similar trends as we apply a bottom gate bias, indicating single carrier transport. We note that similar behaviour has been previously noted in coupled quantum wells^{12,29}. This would also explain why, in Fig. 2c, the Hall mobility follows a simple power law scaling at low carrier densities, as only one carrier gas is present, and the bottom gate thus modulates the density of electron-like states.

To examine further the peak in the Hall mobility at a carrier density of $(15.9 \pm 0.2) \times 10^{11} \text{ cm}^{-2}$, we consider the quantum lifetime as a function of carrier density. The quantum lifetime, τ_q , characterises the single particle momentum relaxation time in 2D transport, which includes all scattering events, in contrast to the classical Drude scattering time, which is weighted towards large angle scattering events. By taking a series of SdH oscillations at a range of temperatures, we can extract the effective mass of carriers (shown in Fig. 4a) and the Dingle ratio (the ratio of the classical Drude scattering time and the quantum lifetime, shown in Fig. 4b)^{26,30}. As we can extract the Drude scattering time from the Hall mobility, we can then use the Dingle ratio to determine the quantum lifetime.

From Fig. 4c we can see that, when the carrier density is low ($n < 12 \times 10^{11} \text{ cm}^{-2}$), the Drude scattering time and the quantum lifetime both increase with increasing carrier density. This is expected, as the screening provided by the 2DEG against scattering events should affect all scattering angles equally, and not just the large angle events that make the largest contribution to the Drude scattering time²⁴⁻²⁶. Subsequently, we find that there is a sudden drop in the quantum lifetime from $0.109 \pm 0.004 \text{ ps}$ to $0.093 \pm 0.004 \text{ ps}$ at a carrier density of $(17.6 \pm 0.2) \times 10^{11} \text{ cm}^{-2}$, followed by an increase in the quantum lifetime, even as the Drude scattering time decreases.

An increase in quantum lifetime as the Drude scattering time falls would imply that low angle scattering events become unfavourable. This can occur if a new subband is populated^{31,32}. Specifically, as a new subband becomes occupied, the states occupying that new subband will screen the system from impurities, as in the single subband case. However, the states occupying this new subband are limited by the subband's size in k -space. There-

fore, the screening provided by this new subband will be greatly reduced if the momentum transferred in a scattering event is greater than $2k_F$, where k_F is the wavevector of the new state at the Fermi energy^{31,32}. The consequence is a selective screening of scattering events, such that events with a small momentum transfer, and thus a small scattering angle, become unfavoured. This results in the observed increase in quantum lifetime.

To confirm the existence of these new states, we took measurements of the transverse magnetoresistance of the coupled quantum well heterostructure at 1.5 K. The current was applied down the x axis, at right angles to the applied magnetic field along the y axis, where z points out of the device plane. It has been previously noted that applying a small magnetic field (3 T) in the plane of a device results in the creation of mid-gap states within an InAs/GaSb quantum well, through moving the InAs dispersion relative to the GaSb dispersion in k ³³⁻³⁵. Additionally, if we consider two sets of states in k -space, one enclosed by the other, an applied magnetic field in the y direction will move the low- k set of states away from $k_x = 0$. This is shown schematically in the inset of Fig. 5b. Eventually, there will come a point where the low- k states are depopulated by the applied magnetic field^{33,36}. This will result in the scattering between the high- k and low- k states becoming suppressed in the x direction, resulting in the observation of a maximum in resistance at zero applied field. We can use this behaviour to extract information about the Fermi surface, as the full-width-at-half-maximum (FWHM) of the $B_{\parallel} = 0$ resistance maximum will be proportional to the Fermi wavevector, k_F , of these low- k states^{37,38}. The in-plane magnetoresistance is, therefore, an extremely sensitive probe of the band structure, as it depends on the availability of states in k -space to act as scattering paths, not the occupation of those states^{33,37,38}.

Fig. 5a shows a series of measurements of the transverse magnetoresistance (magnetic field along the y axis, current applied along the x axis) at a range of top gate biases. We find that, if the top gate bias is more negative than -0.6 V, or more positive than 1.0 V, then the magnetoresistance is approximately parabolic with field. However, between these gate biases, we note that there exists a $B_{\parallel} = 0$ maximum in resistance, indicative of a new set of states available for scattering, that can be easily influenced by an applied magnetic field. When $V_{\text{tg}} = -0.6$ V (at the onset of the $B_{\parallel} = 0$ maximum in resistance), the measured sheet resistance is comparable with that seen at a Hall carrier density of $(14 \pm 1) \times 10^{11} \text{ cm}^{-2}$, in the absence of an in-plane magnetic field. Coincidentally, this carrier density is where the Hall mobility in Fig. 2c starts to deviate significantly from the simple $\mu \propto n^{1.31 \pm 0.05}$

dependence that is seen at low carrier densities.

In order to quantify the extent of these states in k -space, we calculate the FWHM of the $B_{\parallel} = 0$ resistance maximum, and plot this in Fig. 5b as a function of top gate bias. The FWHM is largest when $V_{\text{tg}} = +0.6$ V, where the measured sheet resistance, in the absence of a magnetic field, is comparable with that seen at a Hall carrier density of $(20 \pm 1) \times 10^{11} \text{ cm}^{-2}$. This carrier density corresponds to the carrier density at which the relative magnitudes of the top and bottom gate biases start to effect the electronic transport (as shown in Fig. 2c), and where the envelope function of the SdH oscillations start to change (as shown in Fig. 3a), signalling the occupation of a second, electron-like subband.

These observations raise some interesting questions about the transport throughout this coupled quantum well system. Why do the relative top and bottom gate biases only have different effects on the Hall mobility when a second, electron-like subband is populated, as shown in Fig. 2c? If a second, electron-like subband is populated at a carrier density of $(20.0 \pm 0.2) \times 10^{11} \text{ cm}^{-2}$ (as shown in Fig. 3), what is the significance of the peak in Hall mobility at a carrier density of $(15.9 \pm 0.2) \times 10^{11} \text{ cm}^{-2}$? What is the origin of the states visible in the in-plane magnetoresistance (Fig. 5) and that contribute to the selective screening of low angle scattering events (Fig. 4c)? To discuss this further, we consider the band-structure of this coupled quantum well system, and how it behaves as a gate bias is applied.

III. BAND STRUCTURE OF COUPLED QUANTUM WELLS UNDER APPLIED GATE BIASES

We have shown, through measurements of the Hall mobility, quantum lifetime, and in-plane magnetoresistance that the transport within coupled, InAs/GaSb quantum wells can be described by three regimes. The first of these regimes is the low carrier density regime ($n < 12 \times 10^{11} \text{ cm}^{-2}$), where the scattering is governed by screening from the 2DEG within the InAs layer. This is followed by an intermediate carrier density regime ($12 \times 10^{11} \text{ cm}^{-2} \leq n < 20 \times 10^{11} \text{ cm}^{-2}$), where new states become available for scattering near the Fermi energy, creating a $B_{\parallel} = 0$ maximum in the in-plane magnetoresistance. As these states are populated, a fall in the Hall mobility and a simultaneous rise in the quantum lifetime are observed. However, there is no indication of a new electron-like subband, which would

contribute to SdH oscillations. Finally, at the highest measured carrier densities ($n \geq 20 \times 10^{11} \text{ cm}^{-2}$) two electron-like subbands are visible in the SdH oscillations. In this regime the Hall mobility becomes separately dependent on the top and bottom gate biases, whereas at all lower carrier densities the Hall mobility depends solely on the total Hall carrier density of the system. It is worth noting, however, that the dominant scattering mechanism in all three regimes arises from remote impurities, due to the high $\alpha \geq 10$ Dingle ratio observed (as shown in Fig. 4b)³⁹.

We have established experimentally that the carrier distribution does not transfer between quantum wells on application of either a top or bottom gate bias. Therefore, we are confident that the coupling between the two quantum wells is not changed by these biases and neither well is completely pinched off by these gate biases^{28,40,41}. It is notable that if we apply an extreme, negative top gate bias ($V_{\text{tg}} = -15 \text{ V}$) to our heterostructure and completely deplete the InAs quantum well, we have a residual hole-like carrier density of $(5.21 \pm 0.05) \times 10^{11} \text{ cm}^{-2}$ in the GaSb layer (a full gate sweep is shown in the supplemental material⁴²). This carrier density should be sufficient to screen the InAs layer effectively from the electric field produced by the bottom gate¹⁷. Despite this, it is important to consider what effect a gate bias will have on both quantum wells within the coupled quantum well heterostructure, as the screening provided by 2D carrier gases is not total⁴¹. In order to model this, we consider an effective capacitance model³⁴. This model is discussed in detail within the supplementary material⁴².

The most interesting result of the effective capacitance model arises when we consider the action of a bottom gate on the coupled quantum well heterostructure, shown in Fig. 6, where we have assumed that there is a $17 \times 10^{11} \text{ cm}^{-2}$ carrier density present in the InAs well at zero bias. We find that the bottom gate is much more efficient at modulating the hole gas within the GaSb channel (closer to the bottom gate) than the electron gas within the InAs channel, illustrated in Fig. 6a. However, we only reproduce the observed modulation of the electron-like InAs carrier density if we assume that there is no carrier density present within the GaSb well, as shown in Fig. 6b. In this case there is no quantum capacitance associated with the GaSb channel⁴¹, and so a bottom gate would directly modulate the 2DEG within the InAs channel. However, if this was the case, we would expect an asymmetry in the carrier density as a function of bottom gate bias, as a negative bottom gate voltage would result in a higher density of holes within the GaSb channel, which would screen the InAs

channel from the bottom gate (here assumed to occur around zero bias). This asymmetry is not present in our observations, (Figs 2a and 3d) where the carrier density modulation is consistent with the physical gate-channel separation at all biases.

How then, does the bottom gate modulate the electron-like carrier density at all, given that we see no evidence of electron-hole transport at these gate biases? We attribute the modulation of the carrier density with an applied bottom gate voltage to a change in the band alignment within the coupled quantum well, namely a change in the energy of the anticrossing point as we apply a bias to the GaSb layer¹⁸.

For illustrative purposes, we calculated the electronic dispersion relation within this InAs/GaSb coupled quantum well system, under various bias conditions, using a simplified 3×3 matrix model and present the results in Fig. 7. If we assume, that an electric field (in the form of a bottom gate bias) applied to the GaSb layer is completely screened from the InAs layer, then the electric field will only move the energies of the GaSb hole bands¹⁷. The model, and the assumptions used, are outlined in the supplementary material⁴².

As long as the Fermi energy is mid-conduction band (i.e. the Fermi energy crosses the first, hybridised, electron-like subband E1 but does not cross any states in the highest energy hybridised heavy-hole subband H1), applying a small bias to the bottom gate will move the energy at which the InAs conduction bands anticross the GaSb valence bands¹⁸. For example, if we apply a small negative bottom gate bias (as in Fig. 7a), the electronic dispersion of the GaSb valence bands will move up in energy, as will the point where this dispersion anticrosses the InAs conduction band. This change in energy will result in fewer states being available at the bottom of the hybridised subband, E1. Previously occupied states are now either within the hybridisation gap or form part of H1. Therefore, in the low carrier density regime, a negative bias applied to either gate (as in Figs 7a and 7b) will simply remove electron-like states from the conduction band, and therefore reduce the electron-like carrier density. As the carrier density is reduced, the screening provided by the 2DEG will be similarly reduced, resulting in the behaviour seen in Fig. 2c, where the Hall mobility is dependent on the total carrier density and not the relative top and bottom gate biases.

As we increase the carrier density, we enter the intermediate carrier density regime, where we know that a new set of states become available to act as scattering sites in k -space, initially detected by the emergence of a $B_{||} = 0$ maximum in the in-plane magnetoresistance. As

we move through this regime, screening from these new states begins to affect the quantum lifetime and the Drude scattering time drops. This situation is illustrated by the dispersion relations of the first (E1) and second (E2) electron-like subbands, which are plotted in Fig. 7c, where we show the effect of moving the E1 and E2 bands 50 meV *down* in energy, simulating a small positive top gate bias.

As the second electron-like subband (E2) becomes energetically close to the formerly uncoupled hole dispersion (E1 at $k_{\parallel} = 0$), a new anticrossing gap forms¹⁸. This will mean that, should the Fermi energy be within this new anticrossing gap (as in Fig. 7c), there will be a range of energies where, due to this new anticrossing gap, the second electron-like subband, E2, will be unable to cross the Fermi energy. This additional anticrossing explains why we see vacant states near the Fermi energy in the in-plane magnetoresistance, even though no new states are populated until a much higher carrier density is reached. These vacant states are responsible for the $B_{\parallel} = 0$ maximum seen in Fig 5.

As we increase the carrier density through the peak in Hall mobility, the bottom of the second electron-like subband (E2) eventually crosses the Fermi energy. As it does so, the states at the bottom of that subband will become populated. However, due to the anticrossing shown in Fig. 7c, these states will have the dispersion of a heavy-hole subband, and as such will have poor mobility in comparison to the first electron-like subband (E1), decreasing the total mobility of the system. It is worth emphasising that although these hybridised states at the bottom of E2 have a hole-like dispersion, they are populated by electrons, with a negative charge⁵, and as such we do not see electron-hole transport in our Hall data. Due to this low mobility, however, they do not appear in the SdH oscillations at accessible magnetic fields.

As we enter the high carrier density regime, the second electron-like subband is visible in the SdH oscillations. At this point, the energy of the second electron-like subband has been lowered sufficiently to cross the Fermi energy, as in Fig 8a, where the electron-like bands have been moved 100 meV down in energy, simulating a large, positive, top gate bias. Note that the E1-E2 anticrossing gap still exists (highlighted in Fig. 8b), but since the energies of the electron-like subbands are sufficiently lowered by application of a top gate bias, the Fermi energy now crosses states in E2 with an electron-like dispersion. This will cause the relative movement of states (in k -space) upon application of an in-plane transverse magnetic field to be reduced. Specifically, less magnetic field is required to move H1 in k (localised

within the GaSb layer) relative to E1 when compared to moving E2 in k with respect to E1 (both localised within the InAs layer)^{33–36,43}. As such, the effect of an in-plane magnetic field on the 2D Fermi surface will be diminished in the high carrier density limit, resulting in the observed disappearance of the $B_{\parallel} = 0$ resistance maximum in the high carrier density regime.

Applying a gate bias to the GaSb layer (in our case, a bottom gate bias) will change the energy of the uncoupled hole bands. This will, therefore, move the anticrossing points (in energy and in k) between the heavy hole band (H1) and both the first (E1) and second (E2) electron-like subbands, as in Fig. 7a. By changing the energy at which the anticrossing point between the second electron-like (E2) and heavy hole (H1) subbands occurs, the proportion of states within the second electron-like subband that follow a hole-like dispersion can be altered, which will change the effective mass of the E2 subband. In Fig. 8b the effect of applying a negative gate bias to the GaSb layers while the system is in the high carrier density regime is illustrated. Such a bias moves the dispersion of the uncoupled hole bands higher in energy and as such, increases the contribution the heavy hole subband makes to the dispersion of the second electron-like subband. By including more states with a hole-like dispersion, and as such with a large effective mass⁴⁴, in this second electron-like subband, the mobility of that electron-like subband will decrease. This explains the trend observed in Figs 2b and 2c, where a more negative bottom gate bias results in a lower Hall mobility for identical carrier densities.

IV. CONCLUSIONS

We have investigated the scattering within a double gated InAs/GaSb coupled quantum well heterostructure through magnetotransport measurements within the electron dominated regime. We find that the mobility is independent of the relative top and bottom gate biases up until a carrier density of $(20.8 \pm 0.2) \times 10^{11} \text{ cm}^{-2}$. At this carrier density, a second, electron-like subband starts to be visible in the SdH oscillations. Beyond this point, a more negative bottom gate bias also results in a lower Hall mobility.

We note that a peak in Hall mobility, usually associated with the onset of inter-subband scattering^{12,26,27} occurs at a much lower carrier density, $(15.9 \pm 0.2) \times 10^{11} \text{ cm}^{-2}$, where only one subband appears to be occupied. Analysis of the in-plane, transverse, magnetoresistance,

and the quantum lifetime as a function of top gate bias shows that this peak in Hall mobility is due to the onset of inter-subband scattering between the first electron-like subband and a new, hybridised subband. We therefore conclude that the second electron-like subband hybridises with the highest energy heavy hole subband and forms a new anticrossing gap.

Due to the nature of the anticrossing within these InAs/GaSb coupled quantum wells, the first states populated within this new, hybridised, subband will follow a hole-like dispersion, with a high effective mass and low mobility, and therefore will not contribute to the SdH oscillations at the magnetic fields studied here. It will only be at a higher carrier density, when the Fermi energy crosses a region of the second electron-like subband with an electron-like dispersion, that a second electron-like subband will appear in the SdH oscillations. The effective mass of that second subband can then be controlled by applying a gate bias to the GaSb layer, changing the proportion of that subband that follows a hole-like dispersion, by moving the E2-E1 anticrossing point in energy, as illustrated by Fig. 8b. Thus, we conclude that the bottom gate modulates electron-like carriers within the InAs layer by moving the anticrossing point between the electron-like and hole like subbands in energy and in k . Applying a negative bias across the bottom gate, and thereby moving the energies of the hole bands higher, will result in states being depleted from the InAs subbands, resulting in a modulation in the electron-like carrier density, observed in Fig. 3d. This is contrary to previous assumptions, where the modulation of electron-like carriers by a gate bias applied to the GaSb layer was attributed to insufficient screening provided by the hole gas within the GaSb layer integrated into the coupled quantum well¹³. A similar feature has been observed by Nguyen et al.¹² in a coupled InAs/GaSb quantum well system. In that study, however, the carrier density was modulated solely by action of a bottom gate. Additionally, in Ref. 12, the quantum well studied was formed of a 12.5 nm thick InAs layer grown in direct contact with a 5 nm thick GaSb layer (compared with 15/8 nm InAs/GaSb in our case). They observed two separate peaks in mobility, one at a carrier density of $\approx 14 \times 10^{11} \text{ cm}^{-2}$ and another at $\approx 24 \times 10^{11} \text{ cm}^{-2}$. We reason that the peak in mobility at the lower carrier density is due to the additional anticrossing discussed here, whilst the peak at the higher carrier density is due to the population of a second excited electron subband, as stated in Ref. 12.

In conclusion, we have shown evidence of an E1-E2 hybridisation gap within a InAs/GaSb coupled quantum well. We note that, in our studies, we have not been able to tune the

system into the topologically interesting E1-H1 hybridisation gap. Comparing the E1-E2 hybridisation gap to the E1-H1 hybridisation gap across a series of different quantum well heterostructures would allow one to deconvolute the effects of inter-well coupling (which give rise to both the E1-E2¹⁸ and E1-H1⁵ hybridisation gap) and the excitonic effects recently observed within the E1-H1 hybridisation gap^{1,45}.

V. ACKNOWLEDGEMENTS

We gratefully acknowledge support from the UK Engineering and Physical Sciences Research Council through Grant No. EP/M028143/1, and from the Royal Society through the Wolfson Research Merit Award, No. WM150029.

* C.S.Knox@leeds.ac.uk

¹ L. J. Du, X. W. Li, W. K. Lou, G. Sullivan, K. Chang, J. Kono, and R. R. Du, “Evidence for a topological excitonic insulator in InAs/GaSb bilayers,” *Nat Commun* **8**, 1971 (2017).

² B. Shojaei, A. P. McFadden, M. Pendharkar, J. S. Lee, M. E. Flatte, and C. J. Palmstrom, “Materials considerations for forming the topological insulator phase in InAs/GaSb heterostructures,” *Phys Rev Mater* **2**, 064603 (2018).

³ H. Kroemer, “The 6.1 angstrom family (InAs, GaSb, AlSb) and its heterostructures: a selective review,” *Physica E-Low-Dimensional Systems and Nanostructures* **20**, 196–203 (2004).

⁴ A. Zakharova, S. T. Yen, and K. A. Chao, “Hybridization of electron, light-hole, and heavy-hole states in InAs/GaSb quantum wells,” *Phys Rev B* **64**, 235332 (2001).

⁵ S. de Leon, L. D. Shvartsman, and B. Laikhtman, “Band structure of coupled InAs/GaSb quantum wells,” *Phys Rev B* **60**, 1861–1870 (1999).

⁶ C. L. Kane and E. J. Mele, “Z(2) topological order and the quantum spin Hall effect,” *Phys Rev Lett* **95**, 146802 (2005).

⁷ B. A. Bernevig and S. C. Zhang, “Quantum spin Hall effect,” *Phys Rev Lett* **96**, 106802 (2006).

⁸ C. X. Liu, T. L. Hughes, X. L. Qi, K. Wang, and S. C. Zhang, “Quantum spin Hall effect in inverted type-II semiconductors,” *Phys Rev Lett* **100**, 236601 (2008).

- ⁹ C. Brune, A. Roth, E. G. Novik, M. König, H. Buhmann, E. M. Hankiewicz, W. Hanke, J. Sinova, and L. W. Molenkamp, “Evidence for the ballistic intrinsic spin Hall effect in HgTe nanostructures,” *Nat Phys* **6**, 448–454 (2010).
- ¹⁰ C. Brune, A. Roth, H. Buhmann, E. M. Hankiewicz, L. W. Molenkamp, J. Maciejko, X. L. Qi, and S. C. Zhang, “Spin polarization of the quantum spin Hall edge states,” *Nat Phys* **8**, 485–490 (2012).
- ¹¹ M. Altarelli, J. C. Maan, L. L. Chang, and L. Esaki, “Electronic states and quantum Hall-effect in GaSb-InAs-GaSb quantum-wells,” *Phys Rev B* **35**, 9867–9870 (1987).
- ¹² B. M. Nguyen, W. Yi, R. Noah, J. Thorp, and M. Sokolich, “High mobility back-gated InAs/GaSb double quantum well grown on GaSb substrate,” *Appl Phys Lett* **106**, 032107 (2015).
- ¹³ I. Knez, R. R. Du, and G. Sullivan, “Finite conductivity in mesoscopic Hall bars of inverted InAs/GaSb quantum wells,” *Phys Rev B* **81**, 201301(R) (2010).
- ¹⁴ L. J. Cooper, N. K. Patel, V. Drouot, E. H. Linfield, D. A. Ritchie, and M. Pepper, “Resistance resonance induced by electron-hole hybridization in a strongly coupled InAs/GaSb/AlSb heterostructure,” *Phys Rev B* **57**, 11915–11918 (1998).
- ¹⁵ F. Nichele, A. N. Pal, P. Pietsch, T. Ihn, K. Ensslin, C. Charpentier, and W. Wegscheider, “Insulating state and giant nonlocal response in an InAs/GaSb quantum well in the quantum *hall* regime,” *Phys Rev Lett* **112**, 036802 (2014).
- ¹⁶ W. Pan, J. F. Klem, J. K. Kim, M. Thalakulam, M. J. Cich, and S. K. Lyo, “Chaotic quantum transport near the charge neutrality point in inverted type-II InAs/GaSb field-effect transistors,” *Appl Phys Lett* **102**, 033504 (2013).
- ¹⁷ I. S. Millard, N. K. Patel, M. Y. Simmons, E. H. Linfield, D. A. Ritchie, G. A. C. Jones, and M. Pepper, “Compressibility studies of double electron and double hole gas systems,” *Appl Phys Lett* **68**, 3323–3325 (1996).
- ¹⁸ I. Lapushkin, A. Zakharova, S. T. Yen, and K. A. Chao, “A self-consistent investigation of the semimetal-semiconductor transition in InAs/GaSb quantum wells under external electric fields,” *J Phys-Condens Mat* **16**, 4677–4684 (2004).
- ¹⁹ V. V. R. Kishore, B. Partoens, and F. M. Peeters, “Electronic structure of InAs/GaSb core-shell nanowires,” *Phys Rev B* **86** (2012).

- ²⁰ A. N. Pal, S. Muller, T. Ihn, K. Ensslin, T. Tschirky, C. Charpentier, and W. Wegscheider, “Influence of etching processes on electronic transport in mesoscopic InAs/GaSb quantum well devices,” *Aip Adv* **5**, 077106 (2015).
- ²¹ M. A. Reed, W. P. Kirk, and P. S. Kobiela, “Investigation of parallel conduction in GaAs/Al_XGa_{1-X}As Modulation-Doped Structures in the Quantum Limit,” *Ieee J Quantum Elect* **22**, 1753–1759 (1986).
- ²² J. A. Vanvechten, “Quantum dielectric theory of electronegativity in covalent systems .i. electronic dielectric constant,” *Phys Rev* **182**, 891–903 (1969).
- ²³ E. B. Elkenany, “Theoretical investigations of electronic, optical and mechanical properties for GaSb and AlSb semiconductors under the influence of temperature,” *Spectrochim Acta A* **150**, 15–20 (2015).
- ²⁴ P. J. van Hall, T. Klaver, and J. H. Wolter, “Remote impurity scattering in heterojunctions,” *Semicond Sci Tech* **3**, 120–123 (1988).
- ²⁵ S. Das Sarma and E. H. Hwang, “Universal density scaling of disorder-limited low-temperature conductivity in high-mobility two-dimensional systems,” *Phys Rev B* **88**, 035439 (2013).
- ²⁶ T. Tschirky, S. Mueller, C. A. Lehner, S. Falt, T. Ihn, K. Ensslin, and W. Wegscheider, “Scattering mechanisms of highest-mobility InAs/Al_xGa_(1-x)Sb quantum wells,” *Phys Rev B* **95**, 115304 (2017).
- ²⁷ H. L. Stormer, A. C. Gossard, and W. Wiegmann, “Observation of intersubband scattering in a two-dimensional electron-system,” *Solid State Commun* **41**, 707–709 (1982).
- ²⁸ K. Suzuki, S. Miyashita, and Y. Hirayama, “Transport properties in asymmetric InAs/AlSb/GaSb electron-hole hybridized systems,” *Phys Rev B* **67**, 195319 (2003).
- ²⁹ A. J. A. Beukman, F. K. de Vries, J. van Veen, R. Skolasinski, M. Wimmer, F. M. Qu, D. T. de Vries, B. M. Nguyen, W. Yi, A. A. Kiselev, M. Sokolich, M. J. Manfra, F. Nichele, C. M. Marcus, and L. P. Kouwenhoven, “Spin-orbit interaction in a dual gated InAs/GaSb quantum well,” *Phys Rev B* **96**, 241401(R) (2017).
- ³⁰ Y. F. Komnik, V. V. Andrievskii, I. B. Berkutov, S. S. Kryachko, M. Myronov, and T. E. Whall, “Quantum effects in hole-type Si/SiGe heterojunctions,” *Low Temp Phys+* **26**, 609–614 (2000).
- ³¹ G. Q. Hai, N. Studart, F. M. Peeters, P. M. Koenraad, and J. H. Wolter, “Intersubband-coupling and screening effects on the electron transport in a quasi-two-dimensional δ -doped

- semiconductor system,” *J Appl Phys* **80**, 5809–5814 (1996).
- ³² E. D. Siggia and P. C. Kwok, “Properties of electrons in semiconductor inversion layers with many occupied electric subbands .1. screening and impurity scattering,” *Phys Rev B* **2**, 1024–1036 (1970).
- ³³ M. Karalic, S. Mueller, C. Mittag, K. Pakrouski, Q. S. Wu, A. A. Soluyanov, M. Troyer, T. Tschirky, W. Wegscheider, K. Ensslin, and T. Ihn, “Experimental signatures of the inverted phase in InAs/GaSb coupled quantum wells,” *Phys Rev B* **94**, 241402(R) (2016).
- ³⁴ F. M. Qu, A. J. A. Beukman, S. Nadj-Perge, M. Wimmer, B. M. Nguyen, W. Yi, J. Thorp, M. Sokolich, A. A. Kiselev, M. J. Manfra, C. M. Marcus, and L. P. Kouwenhoven, “Electric and magnetic tuning between the trivial and topological phases in InAs/GaSb double quantum wells,” *Phys Rev Lett* **115**, 036803 (2015).
- ³⁵ X. G. Wu, “Influence of an in-plane magnetic field on the electronic structure of an inverted InAs/GaSb quantum well,” *J Appl Phys* **122**, 225704 (2017).
- ³⁶ J. M. Heisz and E. Zaremba, “Transverse magnetoresistance of GaAs/Al_xGa_{1-x}As heterojunctions in the presence of parallel magnetic fields,” *Phys Rev B* **53**, 13594–13604 (1996).
- ³⁷ O. N. Makarovskii, L. Smrcka, P. Vasek, T. Jungwirth, M. Cukr, and L. Jansen, “Magnetoresistance and electronic structure of asymmetric GaAs/Al_{0.3}Ga_{0.7}As double quantum wells in an in-plane or tilted magnetic field,” *Phys Rev B* **62**, 10908–10913 (2000).
- ³⁸ A. Kurobe, I. M. Castleton, E. H. Linfield, M. P. Grimshaw, K. M. Brown, D. A. Ritchie, M. Pepper, and G. A. C. Jones, “Wave-functions and Fermi surfaces of strongly coupled 2-dimensional electron gases investigated by in-plane magnetoresistance,” *Phys Rev B* **50**, 4889–4892 (1994).
- ³⁹ S. W. Hwang, H. P. Wei, L. W. Engel, D. C. Tsui, and A. M. M. Pruisken, “Scaling in spin-degenerate landau-levels in the integer quantum Hall-effect,” *Phys Rev B* **48**, 11416–11419 (1993).
- ⁴⁰ J. Li, W. Yang, and K. Chang, “Spin states in InAs/AlSb/GaSb semiconductor quantum wells,” *Phys Rev B* **80**, 035303–1– 11 (2009).
- ⁴¹ S. Luryi, “Quantum capacitance devices,” *Appl Phys Lett* **52**, 501–503 (1988).
- ⁴² See Supplemental Material at URL for additional carrier density analysis, details of both the effective capacitance model, and the 3×3 band structure model. The supplemental material contains Refs. 4, 5, 13, 34, 41, 44, and 46,.

- ⁴³ T. Englert, J. C. Maan, D. C. Tsui, and A. C. Gossard, “A study of intersubband scattering in GaAs-Al_xGa_{1-x}As heterostructures by means of a parallel magnetic-field,” *Solid State Commun* **45**, 989–991 (1983).
- ⁴⁴ I. Vurgaftman, J. R. Meyer, and L. R. Ram-Mohan, “Band parameters for III-V compound semiconductors and their alloys,” *J Appl Phys* **89**, 5815–5875 (2001).
- ⁴⁵ X. D. Zhu, J. J. Quinn, and G. Gumbs, “Excitonic insulator transition in a GaSb-AlSb-InAs quantum-well structure,” *Solid State Commun* **75**, 595–599 (1990).
- ⁴⁶ Y. Naveh and B. Laikhtman, “Magnetotransport of coupled electron-holes,” *Europhys Lett* **55**, 545–551 (2001).

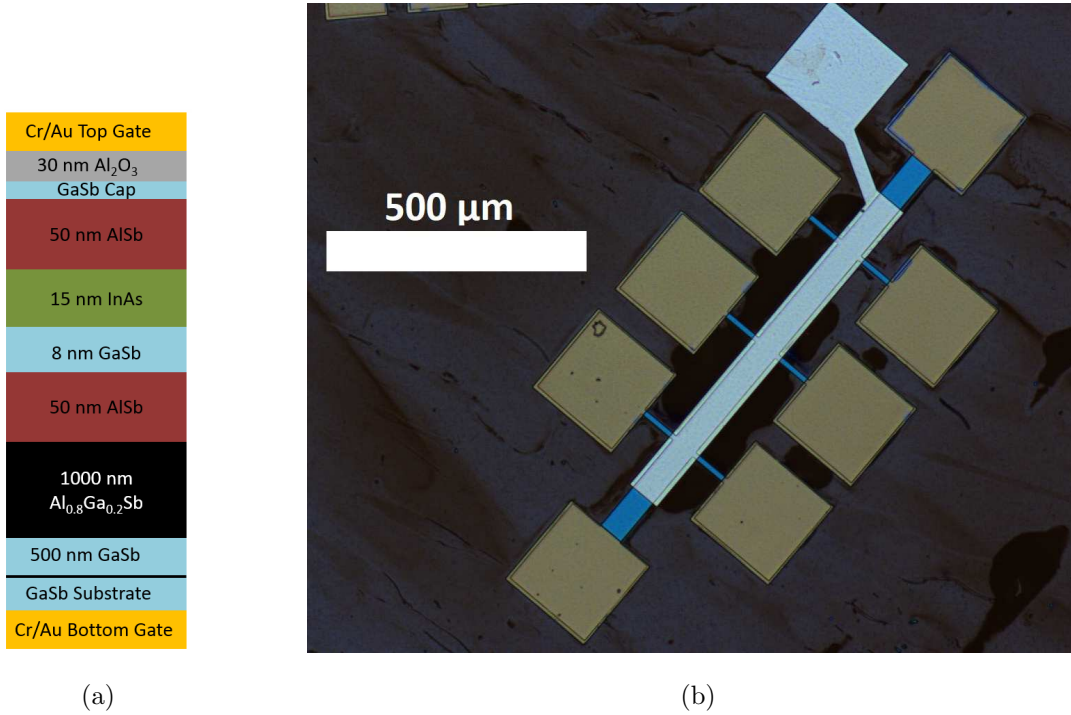


FIG. 1: Sample details for the coupled quantum well structure. The heterostructure design for the wafer is shown in (a). Note that, since the InAs layer is closer to the top surface, the top gate predominantly affects the InAs layer, whilst the bottom gate predominantly affects the GaSb layer. (b) shows an optical micrograph of a typical Hall bar used in this study.

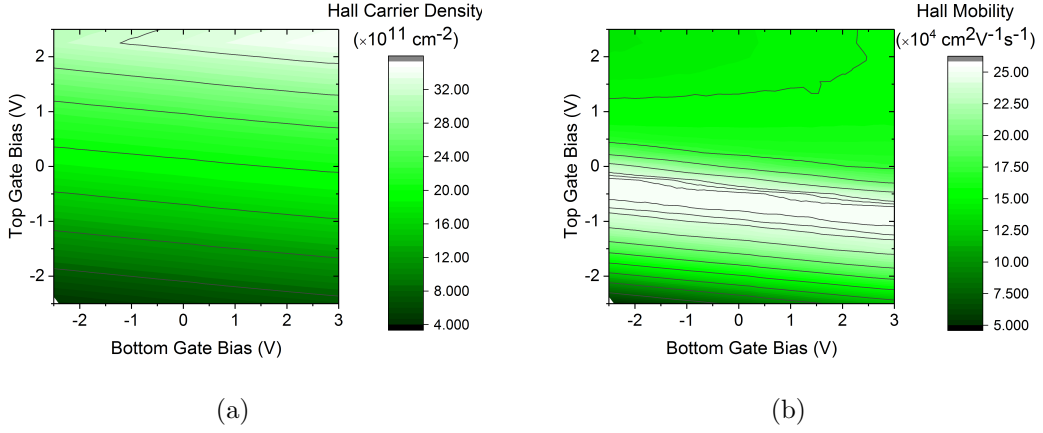


FIG. 2: Dependence of the Hall mobility and carrier density as a function of both top and bottom gate bias. (a) and (b) show contour maps of the Hall carrier density and the Hall mobility, respectively, as a function of both top and bottom gate biases. The black lines indicate contours of constant Hall carrier density and mobility (c) shows the Hall mobility plotted as a function of Hall carrier density, over the same gate bias range in panels (a) and (b). The power law scaling of the mobility, consistent with scattering from remote impurities, is highlighted by the dashed red line.

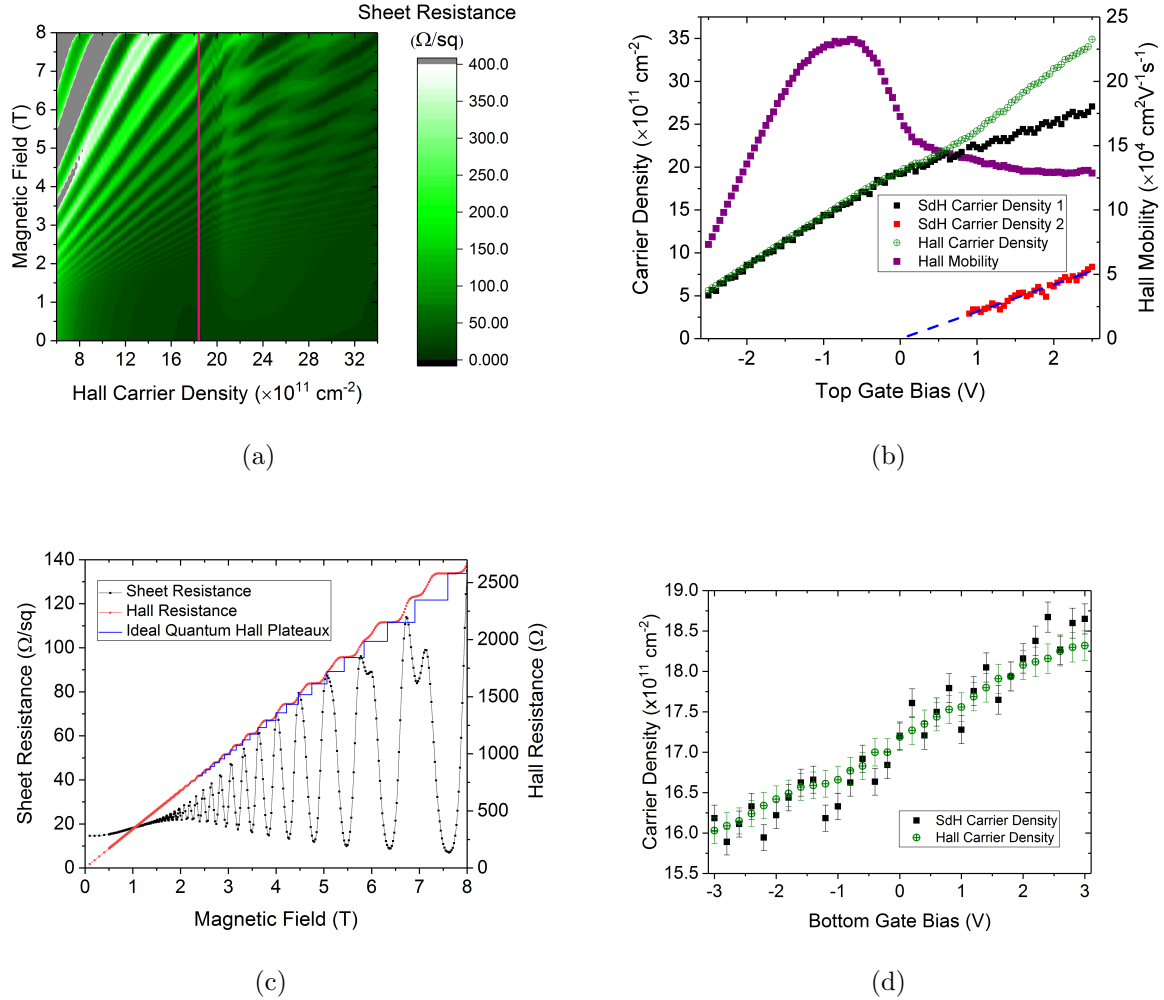


FIG. 3: Analysis of the SdH oscillations at 1.5 K at various gate biases. (a) shows SdH oscillations as a function of Hall carrier density, modulated solely by a top gate bias. (b) shows the carrier densities (black and red) from the Fourier spectrum of the SdH oscillations in (a). The carrier density extracted from the $B \leq 0.2$ T Hall coefficient is also shown (green). The Hall mobility (purple) is plotted for comparison. A linear fit to the 2nd carrier density extracted from the SdH oscillations is also shown by the dashed blue line. For clarity, (c) shows a vertical line section through (a) (highlighted in pink) at a carrier density of $(18.4 \pm 0.2) \times 10^{11} \text{ cm}^{-2}$ (black), with IQHE plateaux measured simultaneously (red), showing transport consistent with a single 2DEG. The expected positions of the IQHE plateaux from the low field Hall coefficient are shown in blue. (d) shows the carrier density from the Fourier spectrum of the SdH oscillations when the carrier density is modulated solely by a bottom gate bias (black). The carrier density extracted from the $B \leq 0.2$ T Hall coefficient over the same gate bias range is also shown (green).

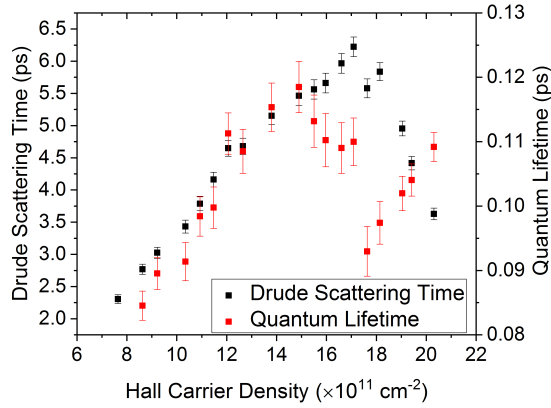
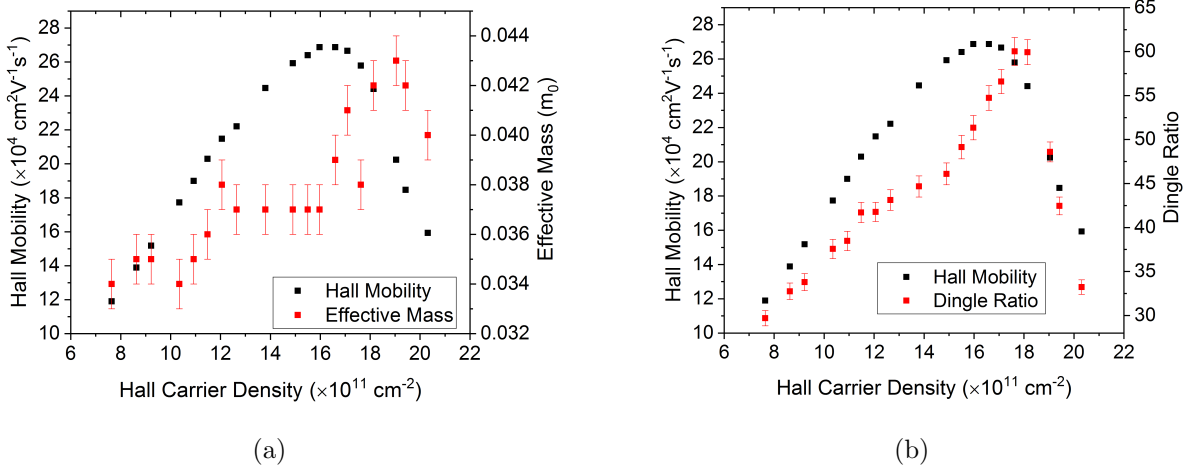


FIG. 4: (a) shows the variation of the effective mass (in units of free electron mass) and Hall mobility (black) with Hall carrier density. (b) shows the variation of the ratio between the Drude scattering time and the quantum lifetime (also known as the Dingle ratio) and Hall mobility (black) with Hall carrier density. (c) shows the Drude scattering time and quantum lifetime as a function of Hall carrier density. The effective mass and Dingle ratio needed to extract this data were derived from fitting the SdH amplitude as a function of temperature up to 20 K at each top gate bias.

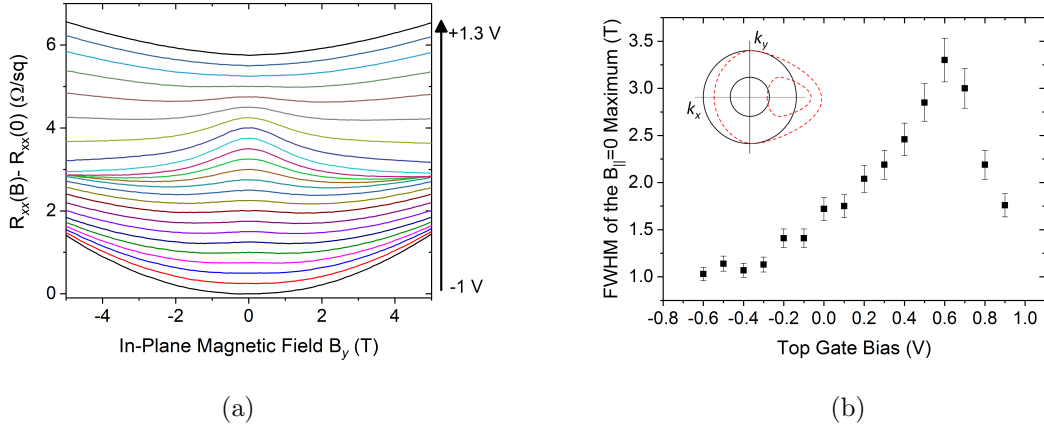


FIG. 5: Analysis of the in-plane magnetoresistance as a function of top gate bias at 1.5 K. (a) shows the transverse magnetoresistance (current along the x axis, magnetic field along the y axis) at a range of top gate biases, with a top gate step size of 100 mV (curves offset for clarity). Note that a $B_{\parallel} = 0$ maximum in resistance starts to form at $V_{\text{tg}} = -0.6$ V, and becomes progressively wider as a more positive top gate bias is applied, until $V_{\text{tg}} = +0.6$ V, where the $B_{\parallel} = 0$ resistance maximum becomes less prominent, before vanishing at $V_{\text{tg}} = 1.0$ V. (b) shows the FWHM of the $B_{\parallel} = 0$ resistance maximum from the relevant curves in Fig. (a). The insert shows a schematic diagram of the 2D Fermi surface, when two states are occupied at zero magnetic field (solid black lines) and on application of an in-plane magnetic field in the y direction (dashed red lines).

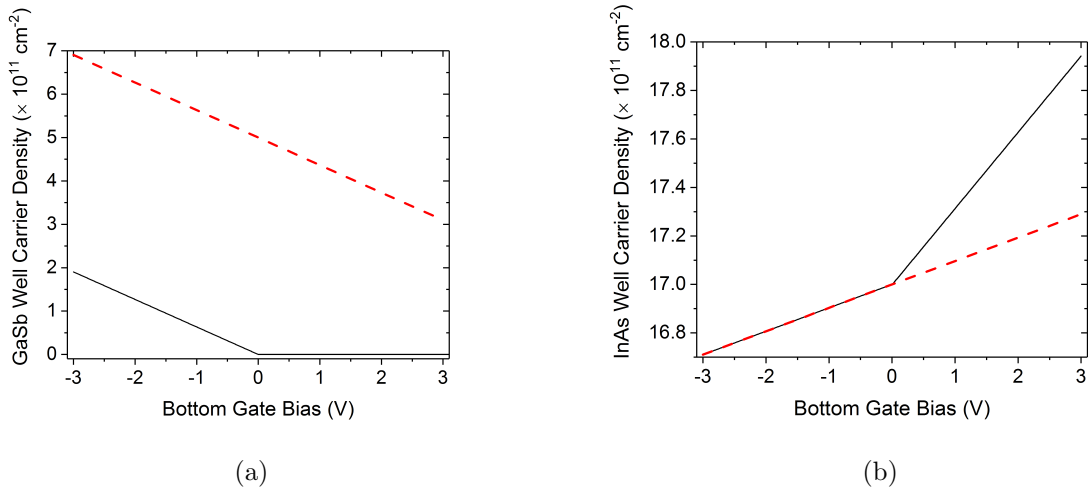


FIG. 6: Calculated carrier densities from the effective capacitance model. At zero gate bias, it is assumed that there is a $17 \times 10^{11} \text{ cm}^{-2}$ carrier density present in the InAs well. The black traces are the results of the model where no carrier density is present in the GaSb well at zero bias, whereas the dashed red traces assume a $5 \times 10^{11} \text{ cm}^{-2}$ carrier density is present within the GaSb well at zero bias. (a) shows the expected carrier density variation within the GaSb channel under a bottom gate bias whereas (b) shows the expected carrier density variation within the InAs channel over the same bottom gate bias range.

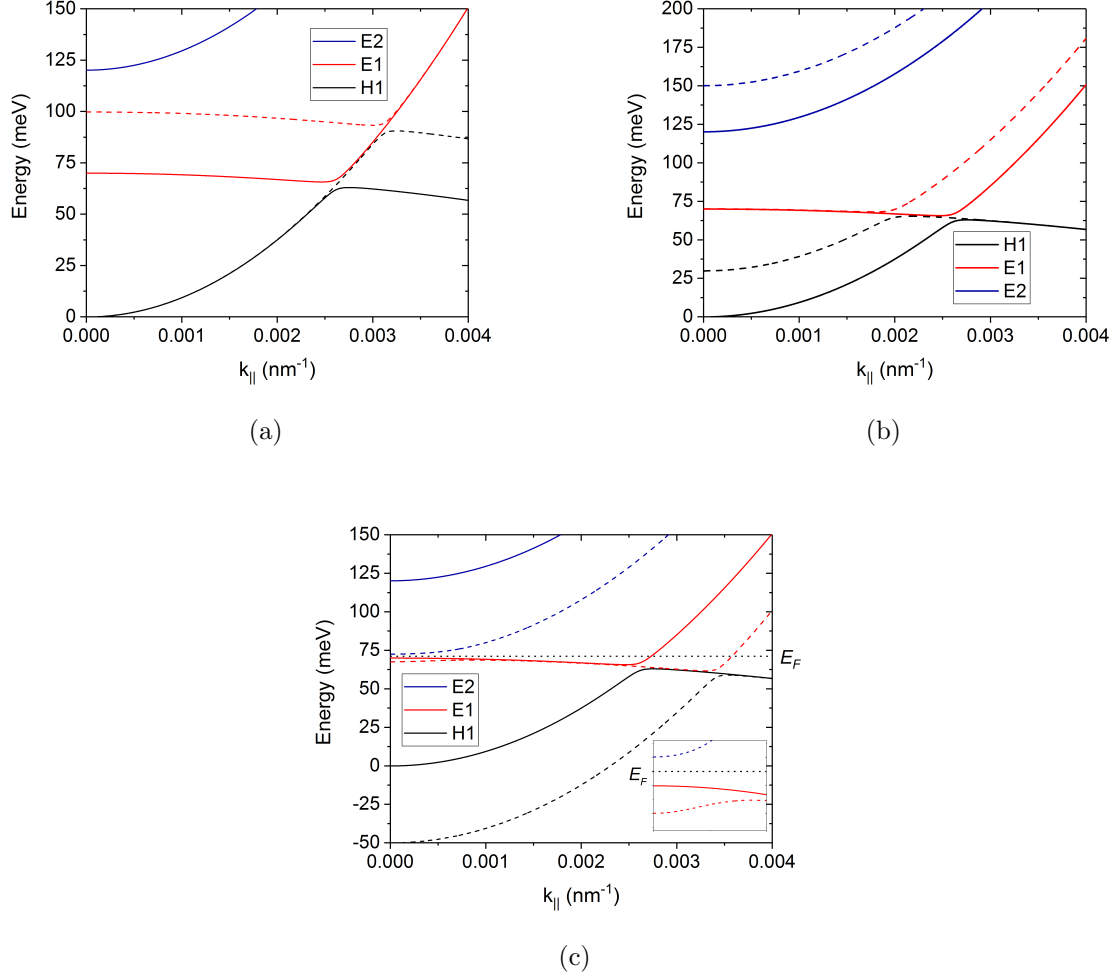


FIG. 7: Illustrative dispersions of the GaSb heavy hole subband (Black, H1), and the first and second electron-like subbands (red, E1 and blue, E2 respectively) under various bias conditions. In all cases, the solid lines represent the system in the low carrier density regime (with the band offsets drawn from Ref 4) and the bottom of the uncoupled InAs conduction band in the absence of a gate bias is set as 0 energy. The dashed traces in (a) show the effect of moving the GaSb dispersions up 30 meV through application of a negative bottom gate bias, compared with the zero gate bias case. For comparison, panel (b) shows the effect of moving the InAs dispersions up 30 meV through application of a negative top gate bias. The dashed traces in panel (c) show the effects of moving the InAs dispersions down 50 meV, displaying the effect of a positive top gate bias. At this point E2 should touch the hybridised portion of E1, but instead a new E2-E1 anticrossing gap is formed, highlighted in the inset. An example Fermi energy is highlighted by the dotted, black line.

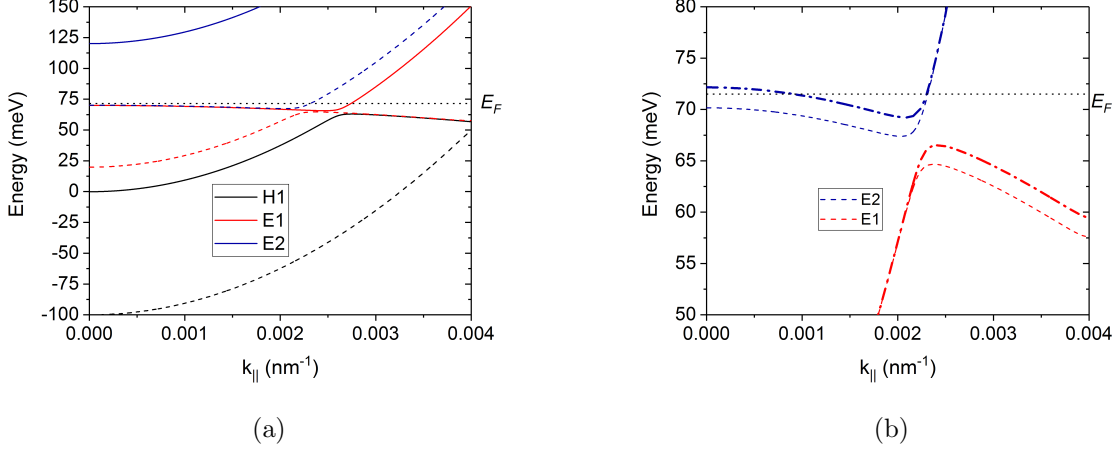


FIG. 8: Illustrative dispersions of the GaSb heavy hole subband (Black, H1), and the first and second electron-like subbands (red, E1 and blue, E2 respectively). The solid lines in panel (a) are identical to the solid lines in Fig. 7. The dashed traces in (a) shows the case in which the InAs dispersions have been moved down 100 meV by application of a large, positive top gate bias in the absence of a bottom gate bias. Note that the E1-E2 anticrossing gap remains, but now the Fermi energy crosses a portion of E2 that has an electron-like dispersion. Panel (b) highlights the E1-E2 anticrossing gap in Fig. (a) without a bottom gate bias (thin trace) and with the GaSb bands moved up 2 meV, simulating a negative bottom gate bias. (thick trace).